

The equatorial Pacific cold tongue simulated by IPCC AR4 coupled GCMs: Upper ocean heat budget and feedback analysis

Yangxing Zheng,¹ Jia-Lin Lin,² and Toshiaki Shinoda³

Received 8 November 2011; revised 4 April 2012; accepted 5 April 2012; published 15 May 2012.

[1] This study examines the contribution of ocean dynamics to sea surface temperature (SST) biases in the eastern Pacific cold tongue region in fifteen coupled general circulation models (CGCMs) participating in the Intergovernmental Panel on Climate Change (IPCC) Fourth Assessment Report (AR4). Twenty years (1980–1999) of the twentieth-century (20C3m) climate simulations from each model are analyzed. An excessive and narrow SST cold tongue that extends too far west into the western Pacific in comparison to observations is a common bias in CGCMs. This feature is found in CGCMs analyzed here and in many previous studies. The heat budget analysis indicates that errors in both net surface heat flux and total upper ocean heat advection significantly contribute to the excessive cold tongue in the equatorial Pacific. The stronger heat advection in the models is caused by overly strong horizontal heat advection associated with too strong zonal currents, and overly strong vertical heat advection due to excessive upwelling and the vertical gradient of temperature. The Bjerknes feedback in the coupled models is shown to be weaker than in observations, which may be related to the insufficient response of surface zonal winds to SST in the models and an erroneous subsurface temperature structure. A hypothesis that describes how the cold tongue bias is possibly developed in the CGCMs is provided based on the results of our analysis.

Citation: Zheng, Y., J.-L. Lin, and T. Shinoda (2012), The equatorial Pacific cold tongue simulated by IPCC AR4 coupled GCMs: Upper ocean heat budget and feedback analysis, *J. Geophys. Res.*, 117, C05024, doi:10.1029/2011JC007746.

1. Introduction

[2] The equatorial Pacific is observed to have a minimum sea surface temperature (SST) that extends from the west coasts of the Americas into the central Pacific. This extension of cool water is commonly referred to as the cold tongue [Wyrki, 1981]. It is generally argued that the Pacific cold tongue is maintained by horizontal advection of cold water from the east and by upwelling of cold water from the subsurface. Net heat flux at the sea surface warms the two contributions. The contributions of cool advection and of upwelling as well as the net surface heat flux vary throughout the year and determine the annual and interannual variations of the cold tongue intensity. Previous studies discussed the relative roles of these contributing terms using large regional box models [Wyrki, 1981; Bryden and Brady, 1985]. For example, Wyrki [1981] suggested from the heat budget analysis that although horizontal advection in the South

Equatorial Current (SEC) contributes to the cold tongue, the contribution from upwelling is much larger. He further indicated that upwelling is limited to relatively shallow depths above the core of the Equatorial Undercurrent (EUC) and the temperatures are around 3°C less than the temperature of the water flowing out laterally. However, Bryden and Brady [1985] found that the zonal and meridional convergences contribute equally to the cold tongue. They also concluded that although the upwelling is large, it contributes little because it occurs in conjunction with the eastward flow of the Equatorial Undercurrent, which shoals to the east and flows predominantly along isotherms. Using data from satellite-tracked drifting buoys and VOS/XBT profiles, Swenson and Hansen [1999] estimated the seasonal cycle of the tropical Pacific Ocean mixed layer heat budget in the cold tongue region and concluded that oceanic heat advection and eddy heat flux convergence play a significant role in the evolution of the Pacific cold tongue.

[3] Besides the contribution of oceanic physical processes as discussed in the above studies, ocean-atmosphere feedback also plays an important role in the formation and maintenance of the Pacific cold tongue. Bjerknes [1969] first hypothesized a positive feedback of tropical ocean-atmosphere interaction that can amplify a perturbation of SST in the cold tongue. The trade winds generate the equatorial upwelling, effectively bringing cold water from the subsurface to the surface to form a cold tongue in the eastern Pacific. Meanwhile, the zonal atmospheric pressure gradient produced by the zonal gradient of the SST drives the Walker

¹Center for Ocean-Atmospheric Prediction Studies, Florida State University, Tallahassee, Florida, USA.

²Department of Geography, Ohio State University, Columbus, Ohio, USA.

³Naval Research Laboratory, Stennis Space Center, Mississippi, USA.

Corresponding author: Y. Zheng, Center for Ocean-Atmospheric Prediction Studies, Florida State University, 2035 E. Paul Dirac Dr., 220C RM Johnson Bldg., Tallahassee, FL 32310, USA. (yzheng@fsu.edu, 850-645-8479)

circulation, which intensifies the surface easterly winds over the Pacific Basin, further strengthening the cold tongue. In this study, we will revisit this feedback in climate models.

[4] It is well known that the Pacific cold tongue plays an important role in the formation of tropical cloud and precipitation patterns, in supplying nutrients for surface ocean biological productivity, and in carbon cycling since it is the major oceanic source of CO₂ for the atmosphere [Field et al., 1998; Calvo et al., 2011]. Large SST anomalies associated with El Niño–Southern Oscillation (ENSO) are manifested as variations about the mean state of the Pacific cold tongue, which affect much of the global climate and weather patterns. Despite its importance in global hydrological and biogeochemical cycles, as well as its influences on global weather and climate patterns, the equatorial Pacific cold tongue has not been well simulated by coupled general circulation models (CGCMs) used for climate predictions and projections [Neelin et al., 1992; Mechoso et al., 1995; Delecluse et al., 1998; Latif et al., 2001; Davey et al., 2002; Meehl et al., 2005; Wittenberg et al., 2006; Dai, 2006; Lin, 2007]. For example, in comparison to observations, an excessive and overly narrow sea surface cold tongue that extends too far west into the western Pacific in the couple climate models has been a common feature for almost two decades [Mechoso et al., 1995; Latif et al., 2001; Randall et al., 2007]. This equatorial Pacific cold bias is usually associated with the double-intertropical convergence zone (ITCZ) problem, which is characterized by excessive precipitation off the equator and insufficient precipitation on the equator in comparison with observations.

[5] The origin of the Pacific cold tongue bias in climate models is complex. Several hypotheses have been proposed to understand the possible causes of the Pacific cold tongue bias. Those possible causes include a wrong deep convection feedback with the planetary boundary layer (PBL) and the SST, wrong solar and longwave cloud forcing, bad coastal winds resulting from coarse resolutions and continental effect, wrong ocean mixing schemes, wrong air-sea interactions giving rise to an improperly stabilized PBL over the cold tongue, large coupling intervals between atmospheric GCM and oceanic GCM, and no biology embedded to affect penetrative radiation in climate models (P. Chang, Summary of the Tropical Bias Workshop, May 28–30, 2003, GFDL, Princeton Univ., Princeton, N. J., available at ftp://grads.iges.org/pub/schneider/CTBW05/Previous_mtg/Ping_CLIVAR_summary.pdf). Consequently, there have been several efforts to reduce the SST bias in the Pacific cold tongue in CGCMs. For example, Yu and Mechoso [1999] reduced this cold tongue bias by imposing an annually varying stratus cloud amount off the Peruvian coast. The bias can also be reduced by refining horizontal and vertical resolutions (C. R. Mechoso, Modeling the southeastern Pacific climate: Progress and challenges, NCEP EMC seminar, 2006; available at <http://www.emc.ncep.noaa.gov/seminars/presentations/2006/Mechoso.NCEP.Jan.06.ppt>), improving the convection scheme [Frey et al., 1997; Zhang and Wang, 2006; Song and Zhang, 2009; Zhang and Song, 2010; Bellucci et al., 2010], and/or changing surface wind stress formulation [Luo et al., 2005] in atmospheric models. It is also believed that ocean–atmosphere feedback plays a critical role in determining the tropical mean climate. The equatorial Pacific cold bias can be moderately reduced by reducing the coupling interval

to three hours in a coupled climate model [Misra et al., 2008]. The ocean–atmosphere feedback in the tropical mean climate system includes the SST gradient–trade wind feedback or Bjerknnes feedback [e.g., Bjerknnes, 1969], the SST–surface latent heat flux feedback [e.g., Wallace, 1992], and the SST–surface shortwave flux feedback [e.g., Ramanathan and Collins, 1991; Peters and Bretherton, 2005]. In fact, many theories have been developed for ocean–atmosphere feedback mechanisms in the coupled tropical mean climate [Neelin and Dijkstra, 1995; Dijkstra and Neelin, 1995, 1999; Sun and Liu, 1996; Jin, 1996; Clement et al., 1996, 2005; Liu, 1997; Liu and Huang, 1997; Clement and Seager, 1999; van der Vaart et al., 2000; Cai, 2003].

[6] Although these previous studies have improved our understanding of the mean climate problem including the equatorial Pacific cold tongue bias, many issues remain unresolved. For example, the contribution of ocean heat advection to the equatorial Pacific cold tongue bias in climate models is still unknown. For the Bjerknnes feedback, previous studies [e.g., Lin, 2007] have examined only the strength of its atmospheric component (i.e., response of winds to SST gradient); none have investigated the strength of its oceanic component (i.e., response of ocean currents and heat advection to surface winds) or the strength of the entire feedback loop, both of which require the calculation of the upper ocean heat budget. Furthermore, Lin [2007] evaluated the response of winds to SST using the atmospheric model simulations forced by observed SST to isolate the possible biases in atmospheric models. However, when the atmospheric models are coupled with ocean models, the wind response to SST may be changed by any biased mean state or by coupling. In this study, we will focus on the equatorial Pacific cold tongue bias by examining the fully coupled simulations of 15 IPCC AR4 CGCMs and directly calculating the upper ocean heat budget and feedback strength. The purposes are threefold:

[7] 1. Examine the structure of ocean circulation and thermodynamics associated with the equatorial Pacific cold tongue bias in CGCMs.

[8] 2. Examine whether ocean heat advection significantly contributes to local SST bias on the equator.

[9] 3. Examine the strength of the entire Bjerknnes feedback loop and its oceanic component in CGCMs.

[10] The remainder of this paper is organized as follows. The models and validation data sets used in this study are described in section 2. The structure of upper ocean circulation in the tropical Pacific is presented in section 3. In section 4 the contribution of ocean heat advection to SST bias in the equatorial Pacific, which is based on an analysis of the upper ocean heat budget, is evaluated. In section 5, the Bjerknnes feedback, including its oceanic component, is discussed. Finally, a summary is presented in section 6.

2. Models and Validation Data Sets

2.1. IPCC Models

[11] The analysis is based on 20-year (1980–1999) model runs of the Climate of the Twentieth Century (20C3M) simulations from 15 coupled GCMs. Table 1 shows the model names and acronyms, their ocean model horizontal and vertical resolutions, the heat flux corrections, and the runs employed for analysis. For each model, we use 20 years of monthly mean ocean temperature, three-dimensional ocean

Table 1. List of 15 IPCC AR4 Coupled GCMs That Participated in This Study

Modeling Groups	IPCC ID (Label in Figures)	Resolution ^a	Heat Flux Correction	Run Number
Canadian Centre for Climate Modeling and Analysis	CGCMA3.1-T47 (cgcm-t47)	192 × 96-L29	Yes	1
Canadian Centre for Climate Modeling and Analysis	CGCMA3.1-T63 (cgcm-t63)	256 × 192-L29	Yes	1
Météo France / Centre National de Recherches Météorologiques	CNRM-CM3 (cnrm)	180 × 170-L33	None	1
CSIRO Atmospheric Research	CSIRO-Mk3.0 (csiro-mk3.0)	192 × 189-L31	None	2
CSIRO Atmospheric Research	CSIRO-Mk3.5 (csiro-mk3.5)	192 × 189-L31	None	1
NASA/Goddard Institute for Space Studies	GISS-AOM (giss-aom)	90 × 60-L31	None	1
NASA/Goddard Institute for Space Studies	GISS-ER (giss-er)	72 × 46-L33	None	1
LASG/Institute of Atmospheric Physics	FGOALS-g1.0 (iap)	360 × 170-L33	None	1
Instituto Nazionale di Geofisica e Vulcanologia	INGV-SXG (ingv)	360 × 180-L33	None	1
Institute Pierre Simon Laplace	IPSL-CM4 (ipsl)	180 × 170-L31	None	1
Center for Climate System Research (The University of Tokyo), National Institute for Environmental Studies, and Frontier Research Center for Global Change	MIROC3.2 –medres (miroc-medres)	256 × 192-L33	None	2
Max Planck Institute for Meteorology	ECHAM5/MPI-OM (mpi)	360 × 180-L40	None	1
Meteorological Research Institute	MRI-CGCM2.3.2 (mri)	144 × 111-L23	Yes	1
National Center for Atmospheric Research	CCSM3 (ccsm3)	320 × 395-L40	None	1
Hadley Centre for Climate Prediction and Research/Met Office	UKMO-HadGEM1 (hadgem1)	360 × 216-L40	None	1

^aResolution is about ocean model output which is denoted by grid points in longitude x latitude and number of vertical layers.

currents, surface wind stress, surface downward/upward shortwave/longwave radiation, surface latent heat flux, and surface sensible heat flux.

2.2. SODA

[12] The Simple Ocean Data Assimilation (SODA) methodology, the ingested data, and the error covariance structure of both the model and the observations are described by *Carton et al.* [2000a, 2000b], *Carton and Giese* [2008], and *Zheng and Giese* [2009]. In this study, SODA v2.0.2 is used. SODA ocean analysis is suitable for evaluating the simulations of CGCMs without assimilating data [*Zheng et al.*, 2011]. The ocean model is based on the Los Alamos implementation of the Parallel Ocean Program (POP) [*Smith et al.*, 1992]. The model resolution is on average 0.4° (lon) × 0.25° (lat) with 40 levels in the vertical. The model is forced with the European Centre for Medium-Range Weather Forecasts (ECMWF) ERA-40 daily atmospheric reanalysis winds [*Simmons and Gibson*, 2002] for the 44-year period from 1958 to 2001.

[13] The model is constrained by abundant temperature and salinity observations using a sequential assimilation algorithm, which is described by *Carton et al.* [2000a, 2000b] and *Carton and Giese* [2008]. Surface heat fluxes are computed from bulk formulae [*Smith et al.*, 1992], using atmospheric variables from the NCEP/NCAR reanalysis [*Kalnay et al.*, 1996]. The NCEP/NCAR reanalysis information is used for the bulk formulae instead of the ERA-40 variables throughout the experiment to give continuity of surface forcing during periods for which the ERA-40 winds are not available. However, the details of the surface heat flux boundary condition are relatively unimportant in influencing the solution, since near-surface temperature observations are used to update the mixed layer temperature. Vertical diffusion of momentum, heat, and salt is based on a nonlocal K-profile parameterization (KPP) [*Large et al.*, 1994] and horizontal diffusion for subgrid-scale processes is based on a biharmonic mixing scheme.

[14] Averages of model output variables (temperature, salinity, and velocity) are saved at five-day intervals. These average fields are remapped onto a uniform global $0.5^\circ \times 0.5^\circ$ horizontal grid using the horizontal grid spherical coordinate

remapping and interpolation package with second-order conservative remapping [*Jones*, 1999].

2.3. Heat Flux Data Set

[15] In this study, monthly mean surface heat fluxes from the Objectively Analyzed air-sea Heat Fluxes Project (OAF flux) [*Yu and Weller*, 2007; *Yu et al.*, 2008] at the Woods Hole Oceanographic Institution (WHOI) are used for evaluating the heat fluxes in CGCMs because they are the latest, and perhaps the best validated data sets. Daily fluxes are computed from the optimally estimated variables using the state-of-the-art Tropical Ocean Global Atmosphere Coupled Ocean-Atmosphere Response Experiment (TOGA COARE) bulk flux algorithm 3.0 [*Fairall et al.*, 2003]. Surface shortwave and longwave radiation of OAF flux is derived from the International Satellite Cloud Climatology Project (ISCCP)-FD estimates [*Zhang et al.*, 2004], which are available from 1 July 1983. These flux estimates are compared to 107 (105 buoys and 2 ships) in situ flux time series, and it is found that they are relatively unbiased and have the smallest mean error compared to other data sets [*Yu and Weller*, 2007; *Yu et al.*, 2008].

3. Structure of Upper Ocean Circulation and Thermodynamics

[16] First we look at the structure of upper-ocean circulation and thermodynamics associated with the equatorial cold tongue bias in the tropical Pacific. To qualitatively depict the bias in the position of the equatorial Pacific cold tongue, the observed and simulated ocean mean state of horizontal distribution, rather than the difference between models and observations, is shown. The cold tongue bias in magnitude is also very important to be quantified, as will be discussed in a later section. Figure 1 shows the spatial distribution of time-mean SST and surface currents in the tropical Pacific from SODA ocean analysis and the 15 IPCC AR4 CGCMs. Errors in ocean surface circulation and SST spatial patterns in models are prominent. For example, compared to observations, the cold tongue in most models is too strong and narrow, and it extends too far west into the western Pacific. Also there are strong westward currents in the central and

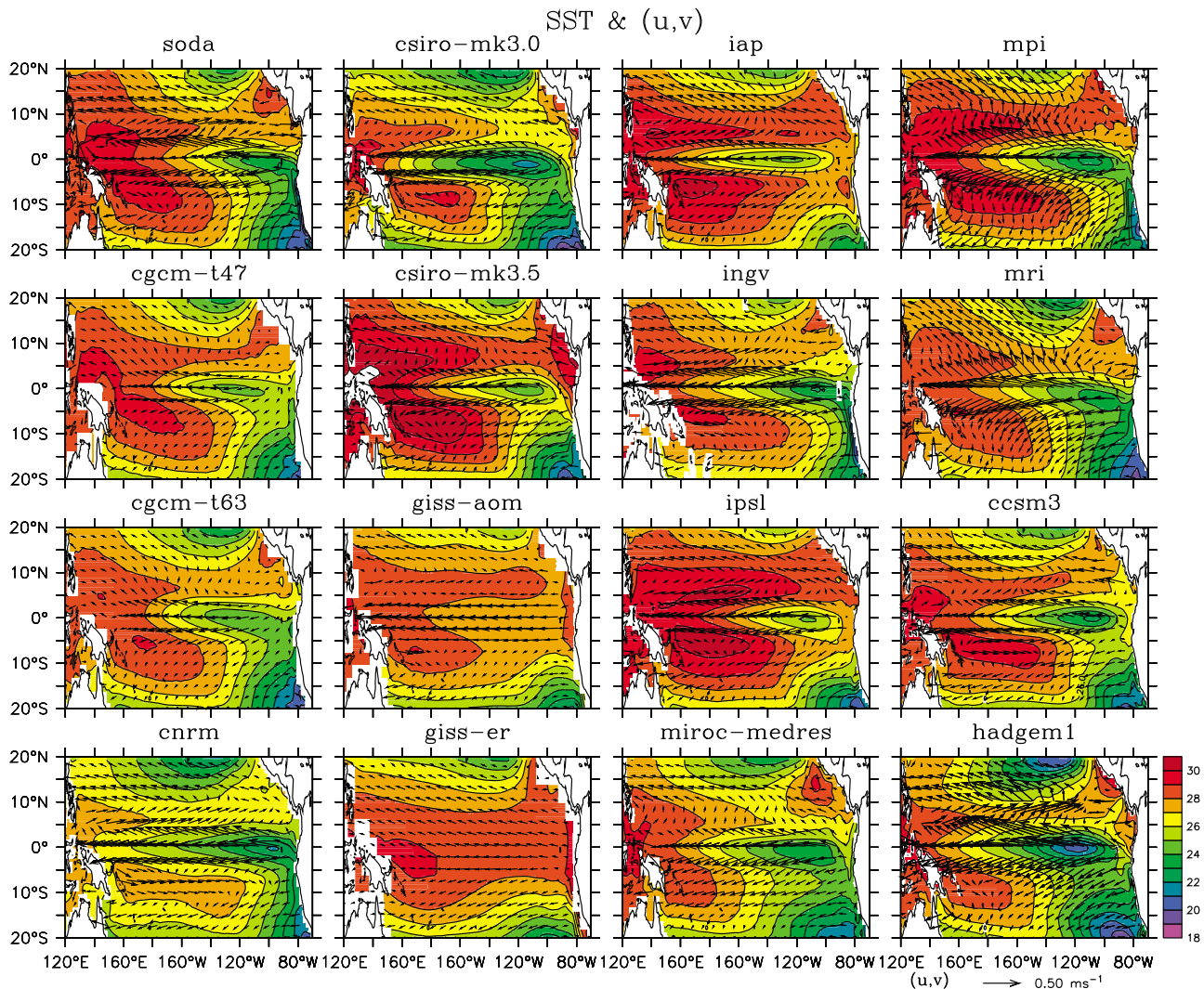


Figure 1. Spatial distribution of time-mean sea surface temperature (SST; shading and contours in $^{\circ}\text{C}$) and surface ocean currents (u,v ; vectors in m s^{-1}) from SODA ocean analysis and 15 IPCC AR4 CGCMs in the tropical Pacific (120°E – 70°W , 20°S – 20°N). The time-mean values are computed by averaging monthly data over January 1980–December 1999. Contour interval for SST is 1°C .

east equatorial Pacific. The cold SST biases in the equatorial central and eastern Pacific may be associated with stronger-than-observed westward surface currents and their associated heat advection along the equator, in addition to coupled processes such as cloud–radiation, wind–evaporation feedback as discussed in detail by Lin [2007].

[17] Figure 2 shows the spatial distribution of annual mean temperature and ocean currents averaged in the upper 50 m in the tropical Pacific Ocean. The spatial pattern in temperature for each model is similar to that for SST in Figure 1 but with a slightly smaller magnitude due to depth averaging; thus, the signature of the cold tongue bias found in the ocean surface is also present in the upper ocean. In the equatorial Pacific, most models produce stronger westward currents than observed that transport water from the cold tongue region to the western warm pool region. Therefore, they may contribute to cold SST bias through overly strong cold advection in addition to equatorial upwelling. Thus, the far westward extension of the cold tongue in most models is associated

with overly strong westward surface and subsurface currents that efficiently bring cold water far westward. Large biases in upper ocean circulation in *giss-aom* and *giss-er* are one of the main causes of large warm SST biases in the entire equatorial Pacific.

[18] Equatorial upwelling is one of the major processes affecting equatorial SST. Similar to Figure 1, ocean mean state on a vertical plane is shown to better qualitatively describe the biases of actual thermocline position and actual vertical circulation in CGCMs compared to observations. Figure 3 illustrates the vertical cross section of annual mean temperature and ocean circulation averaged between 2°S and 2°N . The black curve is the 20°C isotherm, which is in the middle of the equatorial main thermocline. The eastward EUC in the central and east equatorial Pacific is too weak in most CGCMs. Models also have problems simulating the vertical profile of upper ocean temperature. For example, the deepest equatorial thermocline in some models (e.g., *cgcm-t47*, *cgcm-t63*, *csiro-mk3.0*, *csiro-mk3.5*, *miroc-medres*, *mpi*)

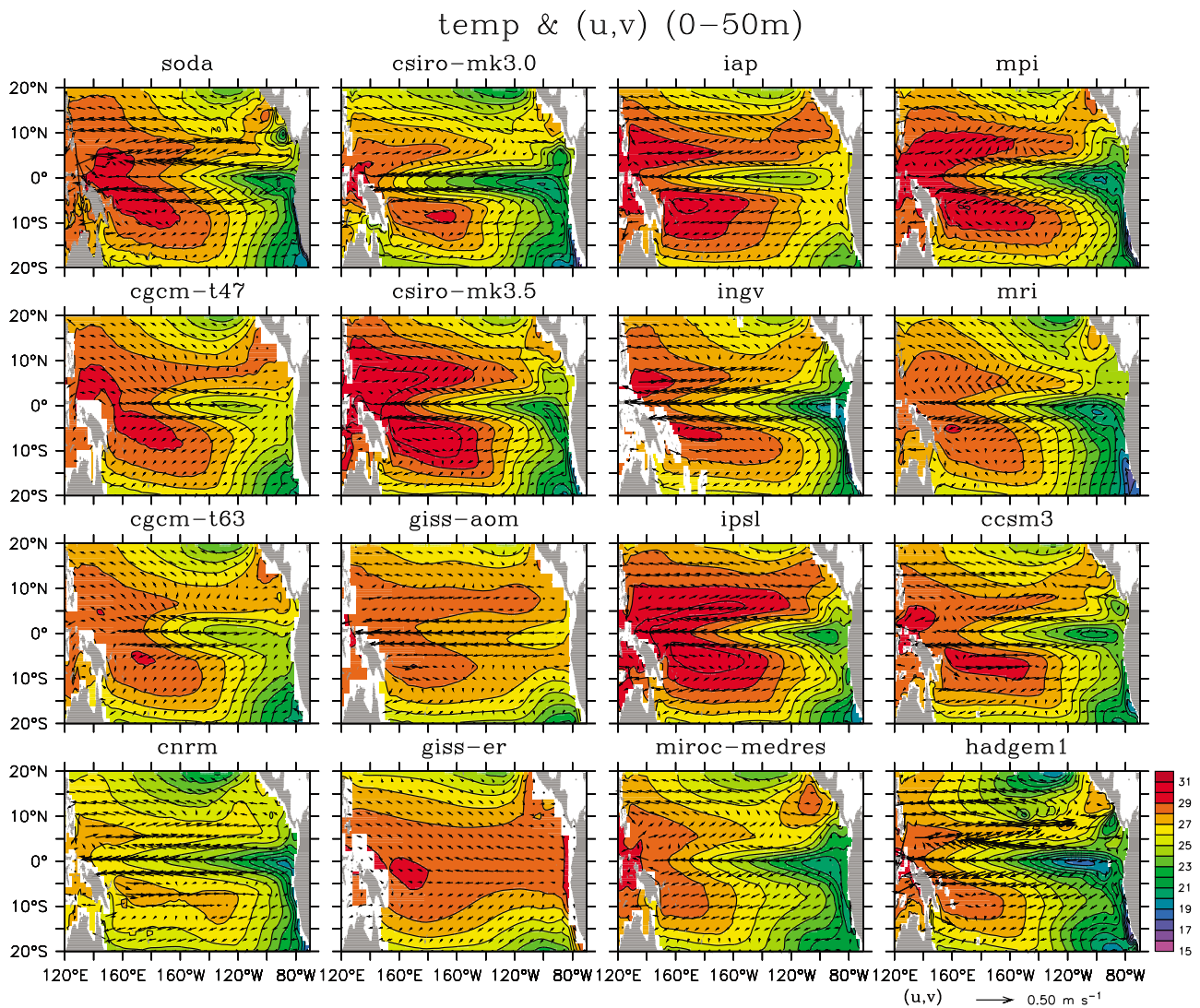


Figure 2. As in Figure 1, but for those averaged in the upper-50-m layer.

is not at the far end of the western Pacific (about 130°E in SODA), but between 140°E and 160°E. Similarly, the shallowest equatorial thermocline in some models is not at the east coastline (around 80°W in SODA) but at around 100°W (e.g., *csiro-mk3.0*, *csiro-mk3.5*, *iap*, *ingv*, *ipsl*, *miroc-medres*, *mpi*, *mri*, *ccsm3*) or around 120°W (e.g., *hadgem1*). Since the thermocline shoals in the eastern Pacific, errors in vertical velocity can produce significant SST biases. The upwelling is too strong between 140°E and 160°W in models such as *cnrm*, *iap*, *ingv*, *mpi* and *hadgem1*, which partly explains the far westward extension of the cold tongue. We will examine upper ocean processes that contribute to errors in the temperature profile and the circulation simulated in these models, particularly in the central and eastern Pacific Ocean. Since temperature in the upper 50 m is a good proxy to time-mean SST, in this study we focus our analysis on the ocean processes in this layer.

4. Upper Ocean Heat Budget Analysis

[19] In this section, we analyze the upper ocean heat budget to understand oceanic processes that could contribute to

the SST bias in IPCC CGCMs. The method for calculating the upper ocean heat budget follows that of *Zheng et al.* [2010, 2011]. Note that CGCMs are not eddy resolved; thus, the eddy heat flux divergence term is not calculated.

4.1. Net Surface Heat Flux

[20] Figure 4 shows the horizontal distribution of net surface heat flux in the entire Pacific from OAFflux and CGCMs that were averaged over the period July 1983–December 1999 (positive values denote warming of the ocean). Note that *ingv* is not included here because surface shortwave and longwave fluxes are not available for this model. Also, note that radiation from ISCCP-FD (and thus net surface fluxes from OAFflux) is available only from 1 July 1983 for the comparison. Most models produce weaker (i.e., less heat input to the ocean) net surface heat fluxes compared to OAFflux in the entire tropical Pacific. The belt of large surface heat flux in the central and eastern Pacific is too narrow in most models, compared with the observation, except for the three models (*cgcm-t47*, *cgcm-t63*, and *mri*) for which heat flux correction was applied. A weak cooling resulting from surface heat flux is present over some regions off the

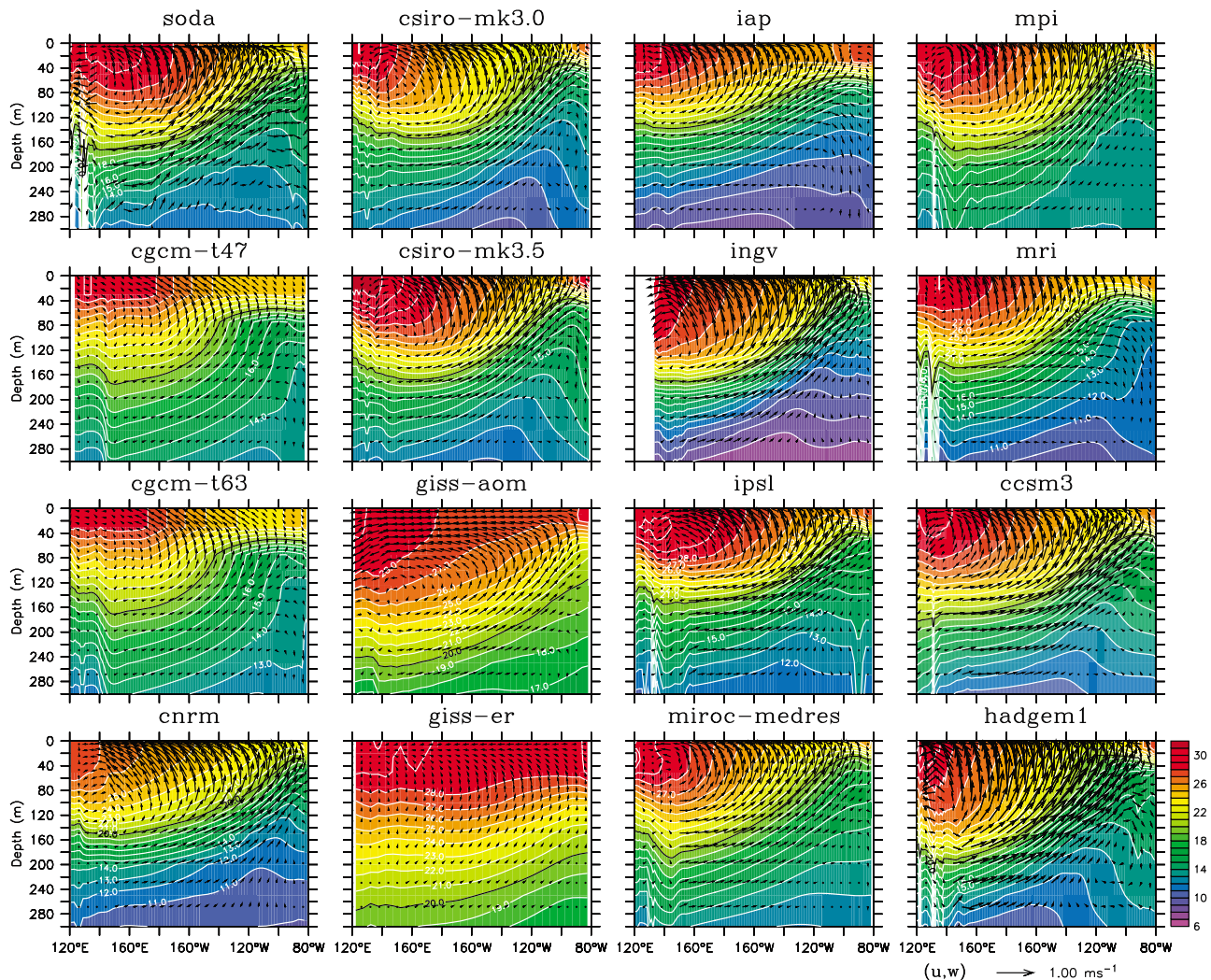
vertical ocean circulation in equatorial Pacific (2°S – 2°N)

Figure 3. Annual mean vertical ocean circulation (vectors in m s^{-1}) and temperature (shading contours in $^{\circ}\text{C}$) in the zonal-vertical plane averaged along 2°S – 2°N from monthly data in SODA ocean analysis and 15 IPCC AR4 CGCMs. 20°C isotherm is denoted by the black curve. The period for averaging is January 1980–December 1999.

equator in all models, whereas in OAFlux there is warming over the entire tropic region. These errors in the net surface heat flux contribute to the SST cold biases along the equator.

4.2. Heat Advection

[21] Total heat advection integrated from the surface to a depth z_0 is defined as

$$H_{adv} = - \int_{z_0}^0 \rho C_p \mathbf{V} \cdot \nabla T dz = - \int_{z_0}^0 \rho C_p \left(u \frac{\partial T}{\partial x} + v \frac{\partial T}{\partial y} + w \frac{dT}{dz} \right) dz,$$

where ρ is the density of seawater; C_p is the specific heat capacity of seawater at constant pressure; \mathbf{V} is the 3D velocity vector, which is $u\mathbf{i} + v\mathbf{j} + w\mathbf{k}$; and u , v , w are their components in zonal, meridional, and vertical direction, respectively. The 3D gradient vector, ∇ , is defined as $\partial/\partial x\mathbf{i} + \partial/\partial y\mathbf{j} + \partial/\partial z\mathbf{k}$. Total heat advection in the upper 50 m

from the 15 IPCC AR4 CGCMs is calculated for the period January 1980–December 1999, and is then compared with the total heat advection from SODA.

[22] Figure 5 shows the spatial distribution of temporal mean total heat advection from the 15 IPCC AR4 CGCMs and SODA. The total heat advection in the upper 50 m contributes to cooling in the equatorial Pacific Ocean in the models and in SODA. In 11 of 15 models (all except *cgcm-t47*, *cgcm-t63*, *giss-aom*, and *giss-er*), the upper-50-m total heat advection contributes more cooling to the equatorial Pacific Ocean than SODA does. Interestingly, in these specific models, an excessive and narrow total heat advection area, extending far west into the western Pacific, is similar to the shape of the cold tongue simulated in the models. The excessive cooling from total heat advection and the insufficient warming from net surface heat flux in most models act together to produce SST cold biases in the equatorial Pacific.

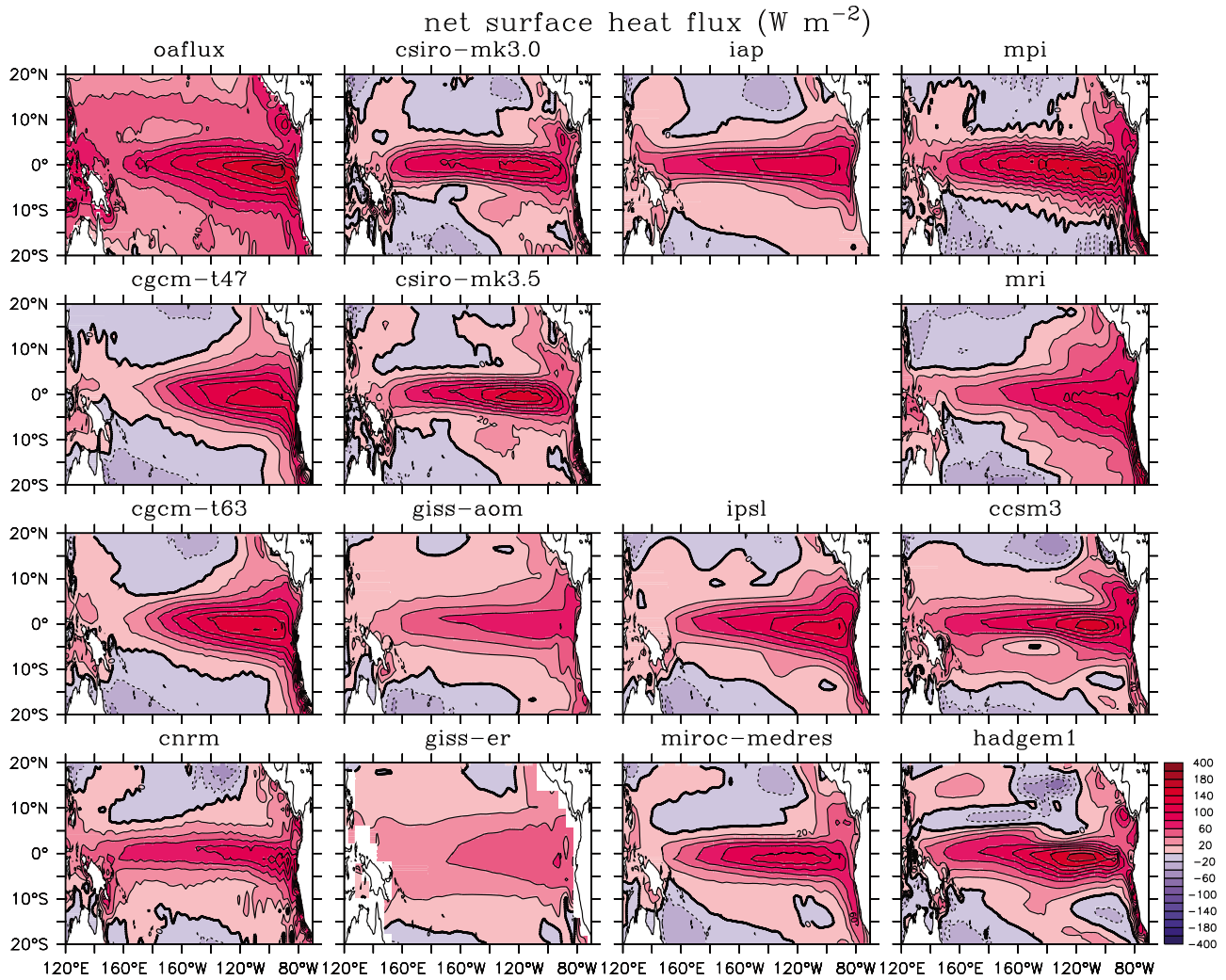


Figure 4. Temporal mean net surface heat flux (W m^{-2}) in the tropical Pacific Ocean from OAFlex and 14 IPCC AR4 CGCMs. The period for averaging is July 1983–December 1999.

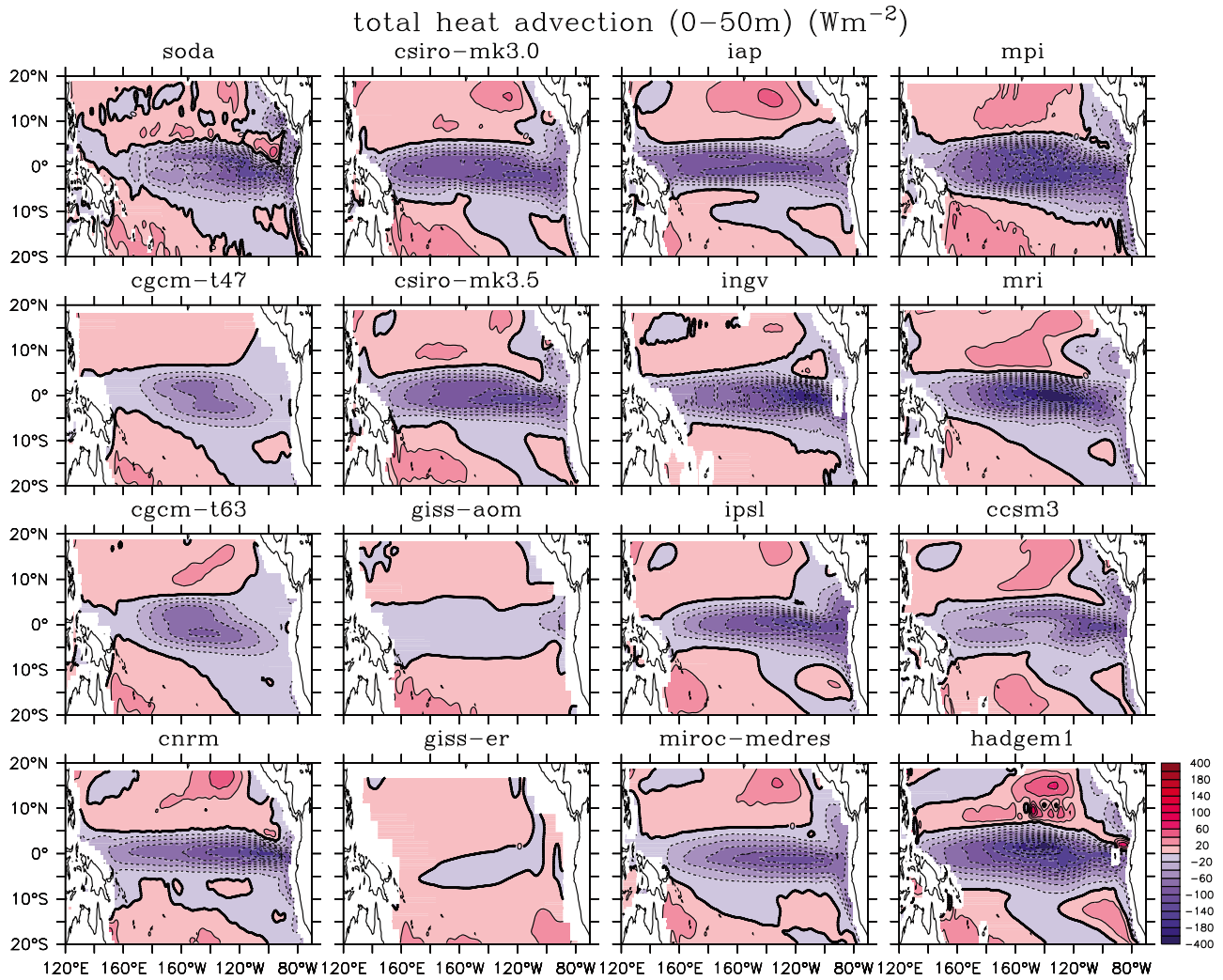


Figure 5. Annual mean total heat advection ($W m^{-2}$) in the upper-50-m layer in the tropical Pacific Ocean from SODA ocean analysis and 15 IPCC AR4 CGCMs. The period for averaging is January 1980–December 1999.

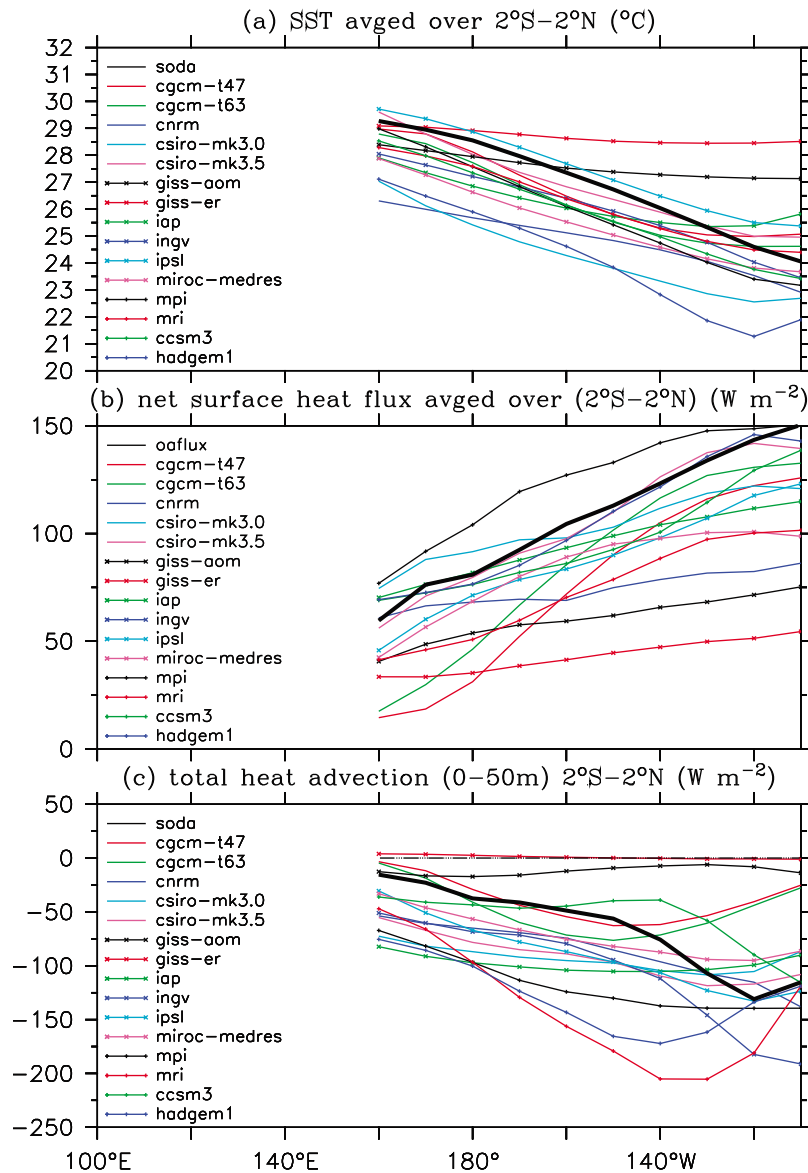


Figure 6. Annual mean (a) SST ($^{\circ}\text{C}$), (b) net surface heat flux (W m^{-2}), and (c) upper-50-m total heat advection (W m^{-2}) averaged along 2°S – 2°N from observed monthly data and 15 IPCC AR4 CGCMs. The data are first converted to 10-degree bins in longitude before meridional averaging. The observed data for SST, net surface heat flux, and zonal wind stress are from SODA ocean analysis, OAFflux, and ERA-40, respectively. The period for averaging is January 1980–December 1999, except for OAFflux, which is averaged over the period January 1984–December 1999.

Therefore, errors in heat advection contribute to the SST cold biases in the equatorial Pacific. It should be noted that the large error in total heat advection from *giss-aom* and *giss-er* is primarily due to the poor simulation of upper ocean circulation (Figures 1 and 2).

[23] Figure 6 displays longitudinal variations of SST, net surface heat flux, and total heat advection that are averaged over the region of 2°S – 2°N for January 1980–December 1999, except for OAFflux, which is averaged over the period from January 1984 to December 1999. Note that the spatial pattern and magnitude of annual mean net surface flux in models averaged over the period January 1984–December 1999 are very similar to those in Figure 6. Figure 6 clearly indicates the quantitative biases in cold tongue SST, net

surface heat flux, and total heat advection in climate models. The unrealistic westward extension of the simulated cold tongue is clearly seen in Figure 6a. Most models generate cold SST biases west of 120°W in the equatorial Pacific, which is associated with insufficient warming from net surface heat flux (Figure 6b) and excessive cooling from total heat advection west of 120°W (Figure 6c).

4.3. Relative Roles of Horizontal and Vertical Heat Advection

[24] Figure 7 shows the horizontal distribution of annual mean horizontal heat advection in the upper 50 m of the tropical Pacific Ocean. The large horizontal heat advection is mostly found between 5°S and 5°N . In the equatorial Pacific

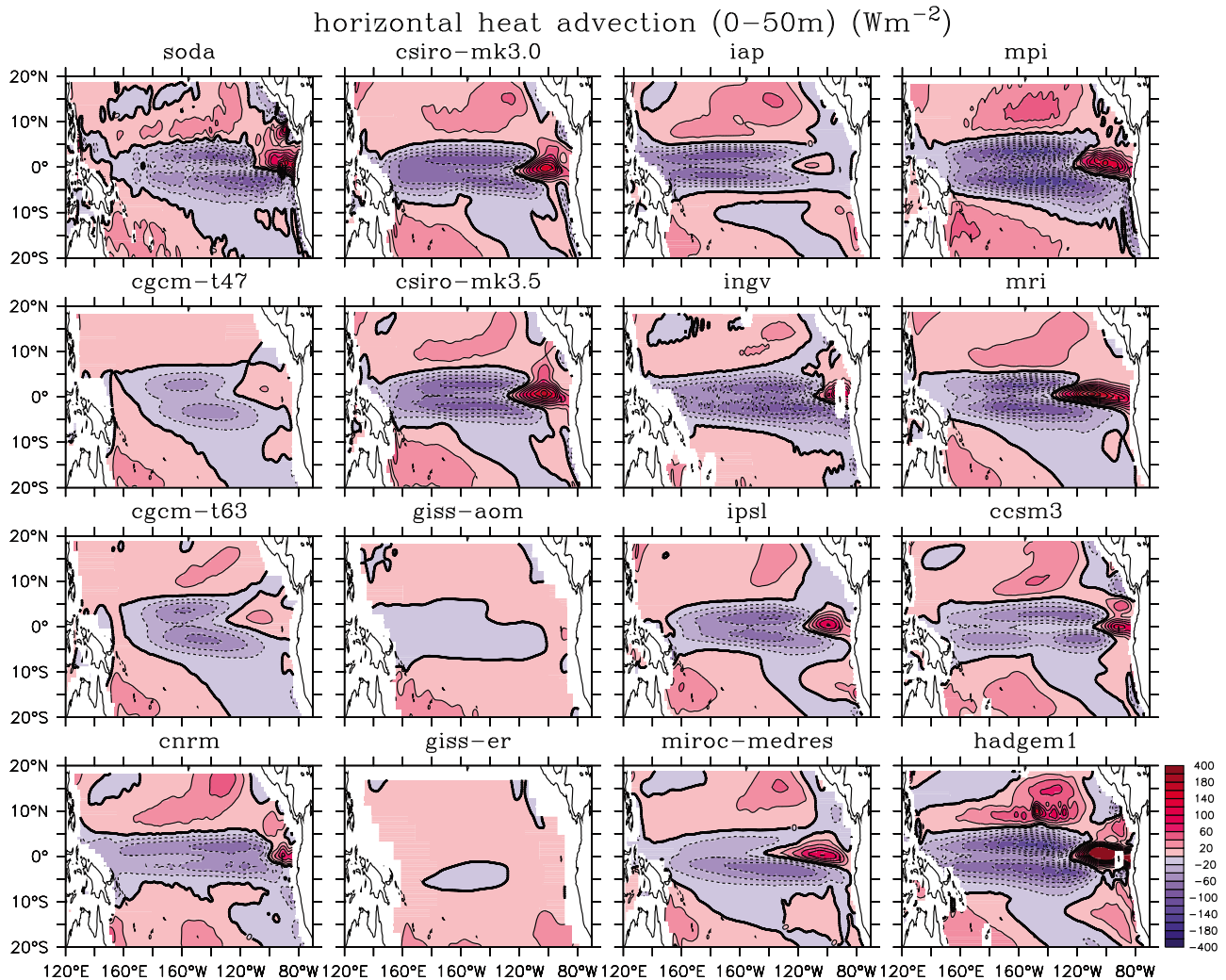


Figure 7. As in Figure 5, but for horizontal heat advection.

there is a dipole-like structure in the horizontal heat advection, and the weakest values are along the equator. Note that horizontal heat advection causes warming in the east equatorial Pacific adjacent to the coast (e.g., east of 100°W).

[25] Figure 8 shows the horizontal distribution of the upper-50-m vertical heat advection. The large vertical heat advection due to equatorial upwelling is mostly found in the eastern Pacific in observations and models. However, the discrepancies between models and observations are prominent. For example, the observed cooling due to strong equatorial upwelling is primarily found east of 140°W , while 11 of 15 models (all except *cgcm-t47*, *cgcm-t63*, *giss-aom*, and *giss-er*) have the area of cooling extending too far west relative to observations.

[26] To examine the relative roles of vertical and horizontal heat advection in the equatorial Pacific Ocean, horizontal and vertical heat advection in the CGCMs is averaged over the region 2°S – 2°N and compared with observations (Figure 9). Warming (up to 75 W m^{-2}) due to horizontal heat advection in the eastern equatorial Pacific adjacent to the coast (east of 120°W) is largely compensated for by cooling (up to 100 W m^{-2}) due to vertical heat advection in models, and thus, the overall cooling of up to -25 W m^{-2} is generated in

this region (Figure 5). However, cooling from vertical heat advection in the central and eastern equatorial Pacific (west of 140°W) is generally weaker than cooling from horizontal heat advection. Note that most models have weaker vertical and horizontal heat advection near the coast relative to SODA. Strong cooling due to horizontal heat advection is found in the eastern and western Pacific whereas the cooling due to vertical heat advection decreases rapidly from east to west. Therefore, the errors of both horizontal and vertical heat advection may contribute to the unrealistic cold tongue simulation. For example, the combined errors of horizontal and vertical heat advection (Figure 6c) cause an excessive cooling up to -75 W m^{-2} in the central and eastern Pacific Ocean.

4.4. Errors in Vertical and Horizontal Heat Advection

[27] Errors in vertical heat advection can be caused by errors in vertical velocity, in vertical temperature gradient, or in both. Figure 10 shows the horizontal distribution of annual mean vertical velocity (upward positive) averaged in the upper 50 m in SODA and in the models. All models except *cgcm-t47*, *cgcm-t63*, *giss-aom*, and *giss-er* generate a narrow latitudinal band (2°S – 2°N) of strong upward velocity. Nine

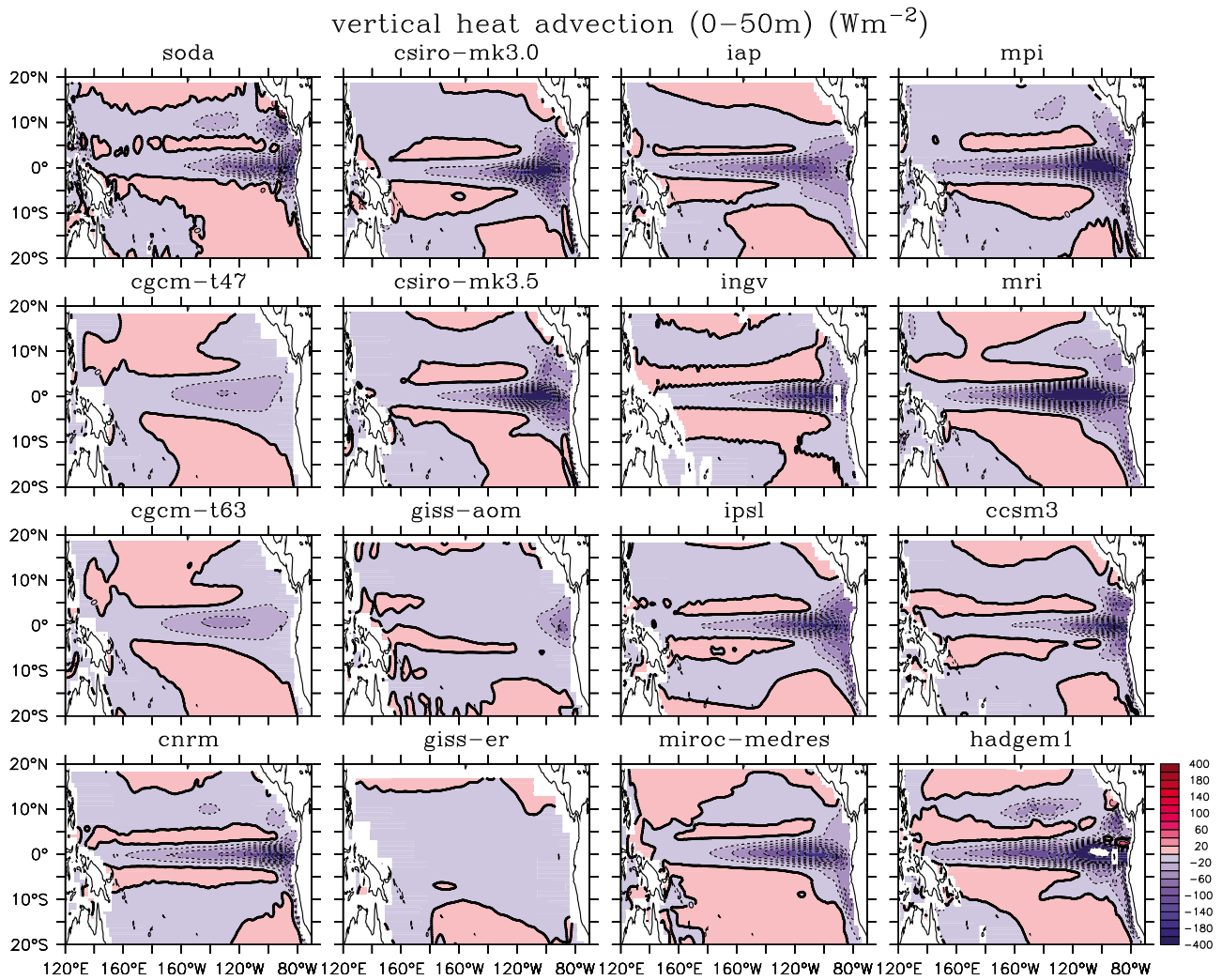


Figure 8. As in Figure 5, but for vertical heat advection.

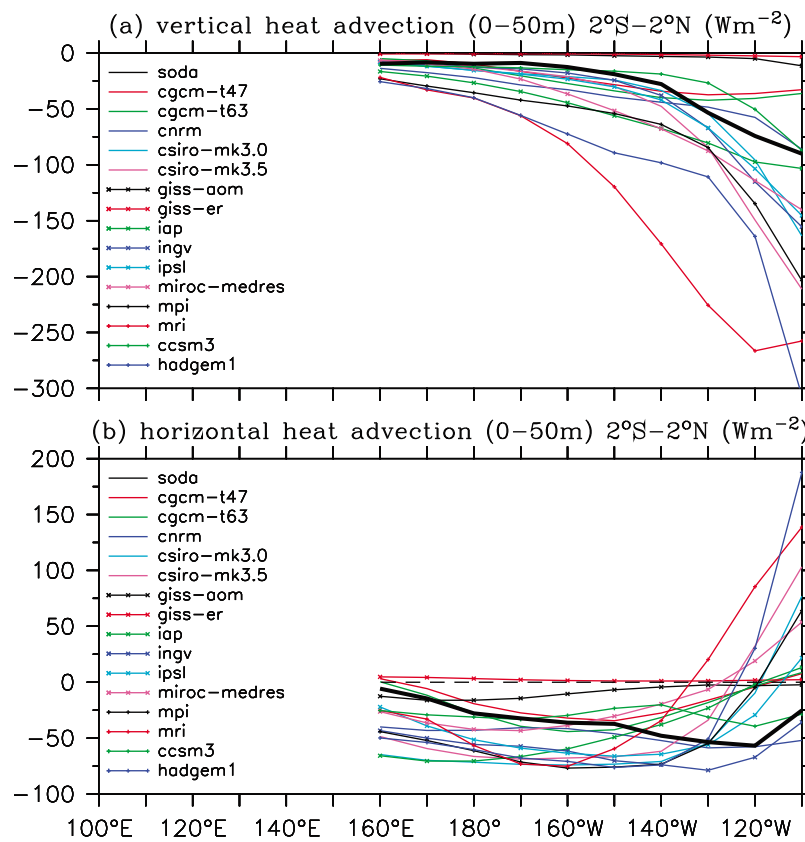


Figure 9. Annual mean (a) vertical and (b) horizontal heat advection (W m^{-2}) in the upper 50 m averaged along 2°S – 2°N from monthly data in SODA ocean analysis and 15 IPCC AR4 CGCMs. The data are first converted to 10-degree bins in longitude before meridional averaging. The period for averaging is January 1980–December 1999.

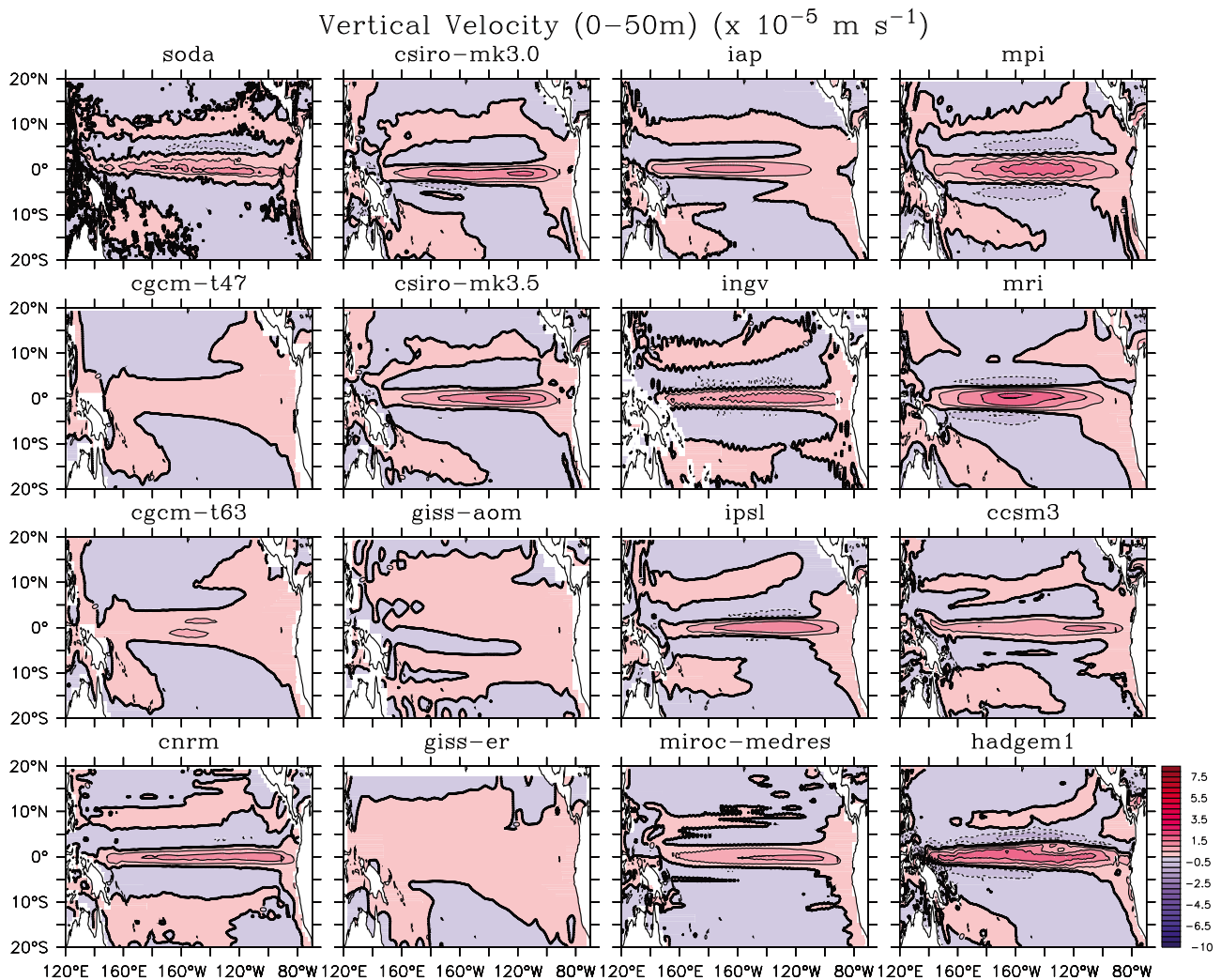


Figure 10. As in Figure 5, but for vertical velocity.

of the above 11 models (i.e., 11 models are all except *cgcm-t47*, *cgcm-t63*, *giss-aom*, and *giss-er*) generate stronger-than-observed upward vertical velocity and the other two models (*iap*, and *ccsm3*) produce a slight weaker upward vertical velocity than observations either in the eastern equatorial Pacific (i.e., *iap*) or in the central equatorial Pacific (i.e., *ccsm3*). Thus, overly strong upward velocity in most models can contribute to the SST cold biases of the equatorial Pacific. Figure 11 shows the horizontal distribution of the annual mean vertical temperature gradient (upward positive) averaged in the upper 50 m in SODA and in the models. The large vertical temperature gradient is mostly confined to the eastern Pacific in SODA and in most models (except *giss-aom* and *giss-er*). In the equatorial Pacific, the large vertical temperature gradient in six models (*csiro-mk3.0*, *csiro-mk3.5*, *ingv*, *ipsl*, *miroc-medres*, and *mpi*) is generally located east of 120°W , similar to the location in SODA. Five models (*cgcm-t47*, *cgcm-t63*, *iap*, *mri*, *hadgem1*) have a large vertical temperature gradient extending west of 120°W along the equator. However, such a large vertical temperature gradient and its westward extension in *cgcm-t47* and *cgcm-t63* do not produce strong cold vertical heat advection because the

vertical velocity is very small (Figure 10). Models such as *giss-aom* and *giss-er* produce weak vertical heat advection owing to small vertical velocity and small vertical gradient of temperature.

[28] Horizontal heat advection near the equator is mainly produced by its zonal component (i.e., $-u\partial T/\partial x$) since zonal circulation dominates along the equator. Figure 12 shows the zonal profiles of annual mean zonal velocity (u), vertical velocity (w), and zonal and vertical gradient of temperature averaged over the region $2^{\circ}\text{S}-2^{\circ}\text{N}$ and in the 0–50-m layer, respectively. It is clearly seen that all models except *giss-er* have westward currents that are too strong in the cold tongue region west of 120°W along with an overly weak zonal gradient of temperature. This indicates that the excessive horizontal cold advection in the cold tongue region west of 120°W (Figure 9) arises largely from the errors of zonal currents, not from the zonal temperature gradient. Eleven of 15 models (all except *cgcm-t47*, *cgcm-t63*, *giss-aom*, and *giss-er*) have overly strong vertical velocity as well as an overly large vertical temperature gradient in the cold tongue extension region. Therefore, both stronger-than-observed vertical velocity and the vertical gradient of temperature play

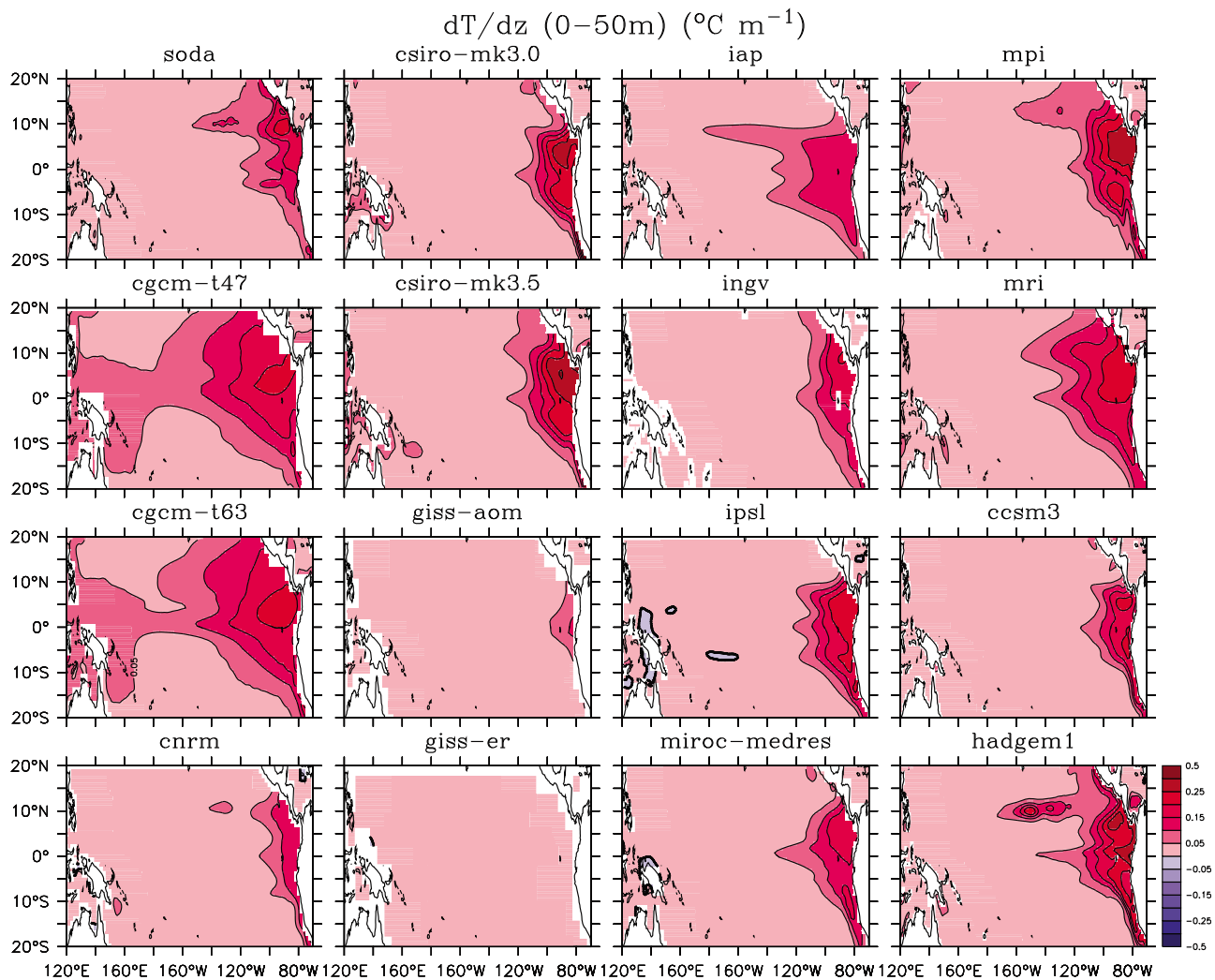


Figure 11. As in Figure 5, but for the vertical gradient of temperature.

an essential role in producing excessive cooling from vertical heat advection, which causes the unrealistic westward extension of the cold tongue.

5. Strength of the Bjerknes Feedback in the Equatorial Pacific Ocean

[29] To discuss the Bjerknes feedback, we use twenty years of monthly time series which contain the variability at all time-scales from two months to twenty years including significant contribution from ENSO-related interannual variability. SST anomaly can affect oceanic heat advection through an atmospheric feedback loop. In particular, SST anomaly influences trade winds, which drive ocean currents and upwelling (downwelling), thus affecting horizontal and vertical heat advection. Heat advection in turn affects SST directly. If there is a linear relationship between SST and heat advection, the SST anomalies can exponentially grow or decay depending on the sign of the regression coefficient. For example, if cold (warm) advection occurs more often during the period of negative (positive) SST anomalies, the cold (warm) SST anomalies are further enhanced. Therefore, the zero-lag linear regression coefficients of heat advection

versus SST can be a measure of the strength of feedback in the coupled system in the equatorial Pacific [e.g., Lin, 2007]. Note that the regression between oceanic heat advection and SST represents the strength of the entire loop of the Bjerknes feedback, including the atmospheric response to SST (not only the oceanic or atmospheric component of the feedback loop).

[30] Here we calculate the linear regression of ocean heat advection versus temperature averaged within 0–50 m (T050), which is a good proxy for mixed layer temperature (or SST) in this region. Figure 13 shows the linear regression of 2°S–2°N averaged of 20-year monthly mean data for the upper-50-m vertical heat advection versus T050 (Figure 13a), horizontal heat advection versus T050 (Figure 13b), and total heat advection versus T050 (Figure 13c). We use the same vertical axis for the three panels to compare the contribution of vertical advection and horizontal advection to the total advection. The analysis of observations indicates that a positive feedback exists between vertical heat advection and T050 in the central and eastern equatorial Pacific Ocean (Figure 13a), between horizontal heat advection and T050 (Figure 13b), and between total heat advection and T050 (Figure 13c). This result can be interpreted as follows.

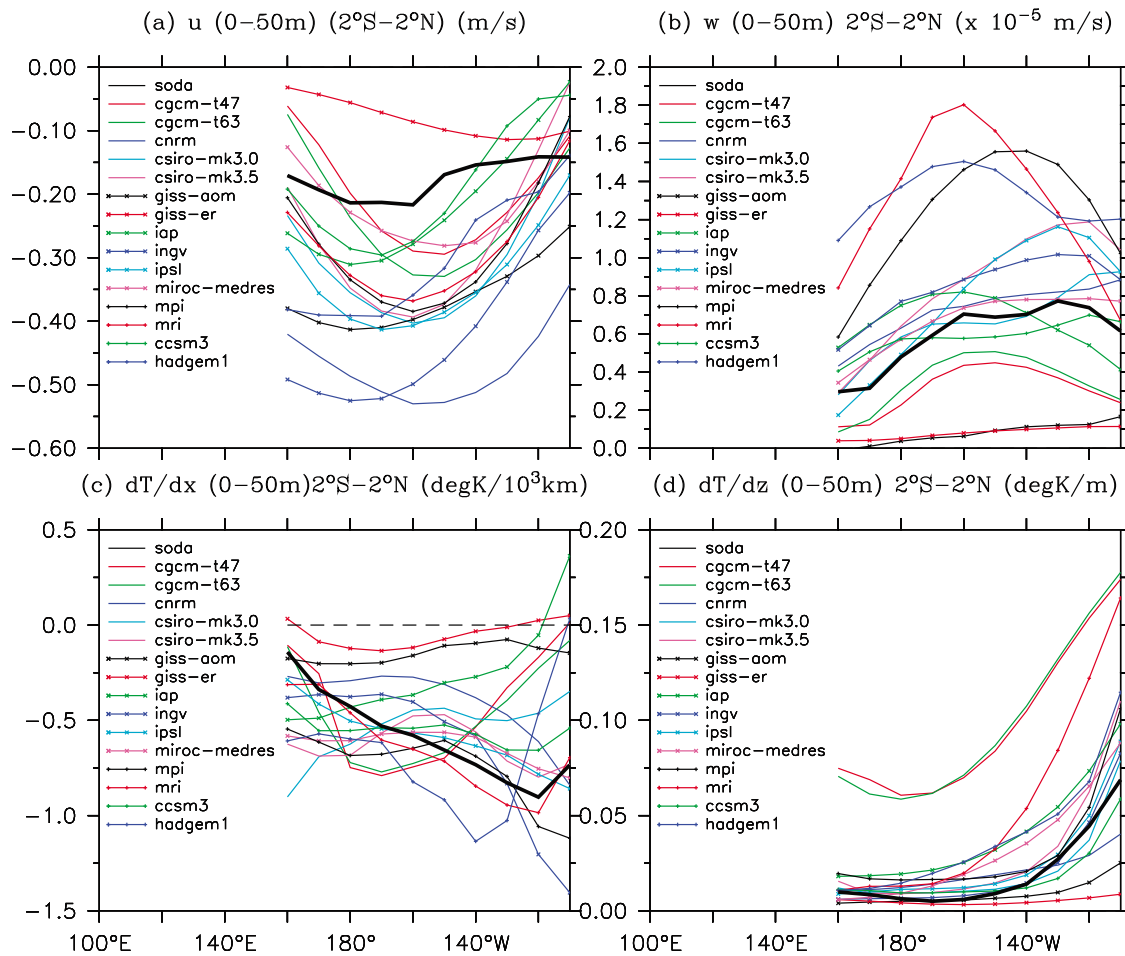


Figure 12. Annual mean (a) zonal velocity (in m s^{-1}), (b) vertical velocity (in 10^{-5} m s^{-1}), (c) horizontal temperature gradient (in $\text{degK per } 10^3 \text{ km}$), and (d) vertical temperature gradient (degK m^{-1}) in the upper 50 m averaged along 2°S–2°N from monthly data in SODA ocean analysis and 15 IPCC AR4 CGCMs. The data are first converted to 10-degree bins in longitude before meridional averaging. The period for averaging is January 1980–December 1999.

An increase in SST in the eastern equatorial Pacific causes a weaker zonal SST gradient between the east and west that results in a weaker zonal wind stress. The weaker zonal wind stress generates a weaker equatorial upwelling and zonal current, and thus decreases the cooling caused by horizontal and vertical heat advection, leading to a further increase in the SST. Because of this (Bjerknes) feedback loop, SST anomalies are enhanced in the coupled system.

[31] An interesting result from the analysis of observations is that the horizontal heat advection, which is dominated by its zonal component, contributes more than the vertical advection does to the total advection. This can be understood from the thermal structure of the upper ocean in the central and eastern equatorial Pacific (Figure 3). In this region, the upper ocean isotherms are tilted with longitude: the 20°C isotherm is about 160 m deep at the dateline and about 50 m deep at 90°W. The tilt of the isotherm means a significant zonal temperature gradient and thus a substantial zonal heat advection by the zonal current. The traditional definition of Bjerknes feedback considers only vertical heat advection, but Figure 13 shows that zonal heat advection plays a more

important role. Therefore, the total heat advection should be considered in discussions of Bjerknes feedback.

[32] Almost all models produce a positive feedback between total heat advection and T050 (Figure 13c), i.e., a positive Bjerknes feedback. However, the models tend to underestimate the strength of Bjerknes feedback over the eastern equatorial Pacific between 150°W and 110°W, which is a key region for the cold tongue and ENSO. Biases in both the vertical advection (Figure 13a) and horizontal advection (Figure 13b) contribute to this bias. It should be noted that the results are similar if SST, instead of T050, is used to calculate the regression (not shown). The overly weak Bjerknes feedback in CGCMs is somewhat surprising, as it seems inconsistent with the excessive cold tongue in those models. We will discuss this issue further in section 6.

[33] The overly weak Bjerknes feedback in CGCMs could be caused by many different factors that are difficult to isolate in the coupled system. Here we only look at some key physical relationships in the models that we hope we can provide some insights into the cause of the problem. For example, the regression between subsurface temperature and

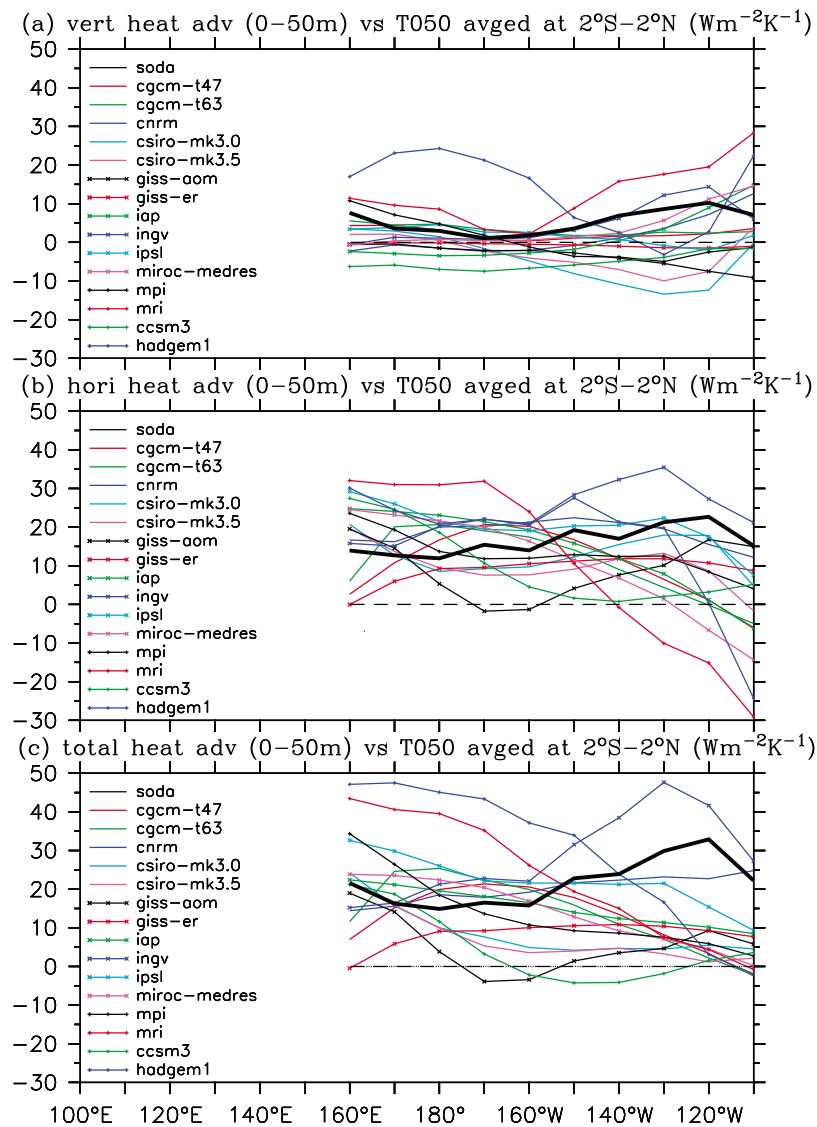


Figure 13. Linear regression of 2°S – 2°N averaged of 20-year monthly mean data for (a) vertical heat advection (0–50 m) vs T050, (b) horizontal heat advection (0–50 m) vs T050, (c) total heat advection (0–50 m) vs T050 ($\text{W m}^{-2} \text{K}^{-1}$) from monthly data in SODA ocean analysis and 15 IPCC AR4 CGCMs. The data are first converted to 10-degree bins in longitude before meridional averaging. The period for analysis is January 1980–December 1999.

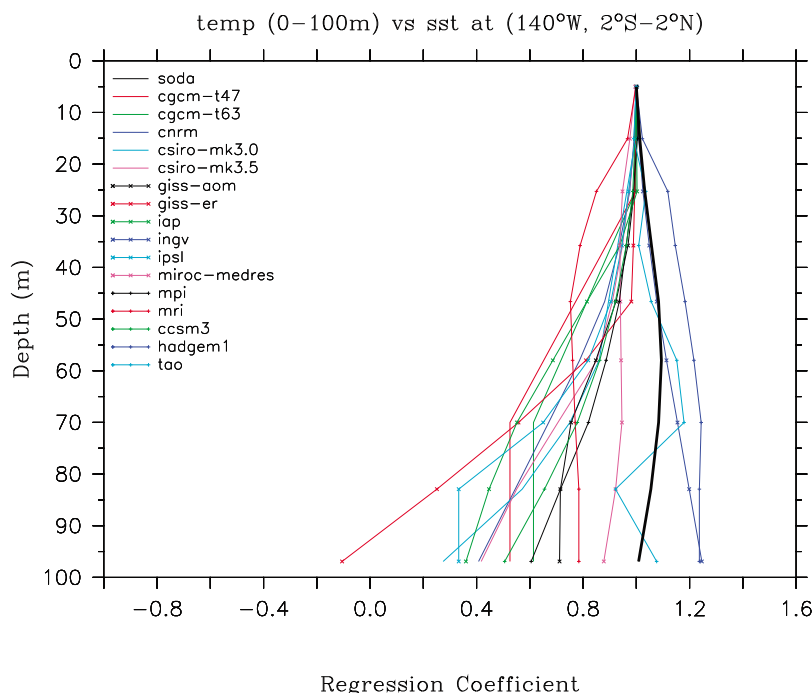


Figure 14. Linear regression of 2°S – 2°N averaged of 20-year monthly mean temperature at 140°W vs SST from monthly data in SODA ocean analysis, TAO buoy data, and 15 IPCC AR4 CGCMs. The data are first converted to 10-degree bins in longitude before meridional averaging. The period for analysis is January 1980–December 1999. TAO buoy data from January 1985–December 2010 are used.

SST at 140°W (Figure 14) shows that subsurface warming (cooling) is generally larger than surface warming (cooling) in the observations, whereas subsurface warming (cooling) is smaller than surface warming (cooling) in most models. The above difference in subsurface temperature structure between models and observations influences the relationship between SST, dT/dz , and vertical heat advection, possibly giving rise to an unrealistic Bjerknes feedback. For example, when the same cold SST anomalies are found in models and observations, the cold anomalies of subsurface temperature tend to be smaller in models than in the observations, leading to an unrealistic vertical temperature gradient with a sign opposite to that in the observations. This incorrect vertical temperature gradient anomaly, when combined with the time-mean upwelling, contributes to the weaker positive or even negative vertical heat advection (as seen in Figure 13a) and therefore weakens the Bjerknes feedback. Figure 15 shows the linear regression of surface zonal wind stress versus T050 (Figure 15a) and depth-averaged vertical velocity versus surface zonal wind stress (Figure 15b). The analysis reveals that the zonal wind stress responds insufficiently to the mixed layer temperature (and thus SST) anomaly in most models (Figure 15a). This, in combination with the overly small time-mean zonal temperature gradient in most models (Figure 12c), tends to produce insufficient zonal heat advection (a dominant component of horizontal heat advection) anomaly associated with SST anomaly (Figure 13b). Therefore, it may contribute to the overly weak Bjerknes feedback in the models. As shown in Figure 18a of Lin's [2007] study, the zonal wind stress responds excessively to the SST in the atmospheric models when forced by the observed SST (without coupling to an ocean model). The

weak response of surface winds to T050 (and SST) in the coupled models suggests that coupling to an ocean model and the resultant overly cold equilibrium SST along the equator (the excessive cold tongue) significantly reduces the excessive response of zonal winds to SST anomaly.

[34] Figure 15b shows that most models produce excessive upwelling (downwelling) anomalies (i.e., more negative values) in the eastern Pacific in response to enhanced (reduced) surface easterly wind stress. This, in combination with the overly large time-mean vertical temperature gradient in most models (Figure 12d), tends to produce excessive vertical heat advection. Therefore, the insufficient response of vertical heat advection to mixed layer temperature or SST in most of the models shown in Figure 13a is not caused by problems in the ocean dynamical upwelling processes (i.e., response of ocean vertical flow to zonal wind stress), but more likely by other processes such as the insufficient surface wind response to SST anomaly (Figure 15a) and the erroneous subsurface temperature structure (Figure 14).

6. Summary

[35] In this study, upper ocean processes in the tropical Pacific are examined in coupled models as a means of increasing our understanding of the equatorial Pacific cold tongue bias. Our analysis indicates that the error of ocean heat advection contributes significantly to the cold SST biases along the equator. Most CGCMs produce overly strong total (horizontal plus vertical) heat advection along the equator (Figure 6c). This is caused by overly strong horizontal advection of heat (Figure 9b) due to overly strong zonal currents (Figure 12a) and by overly strong vertical cold

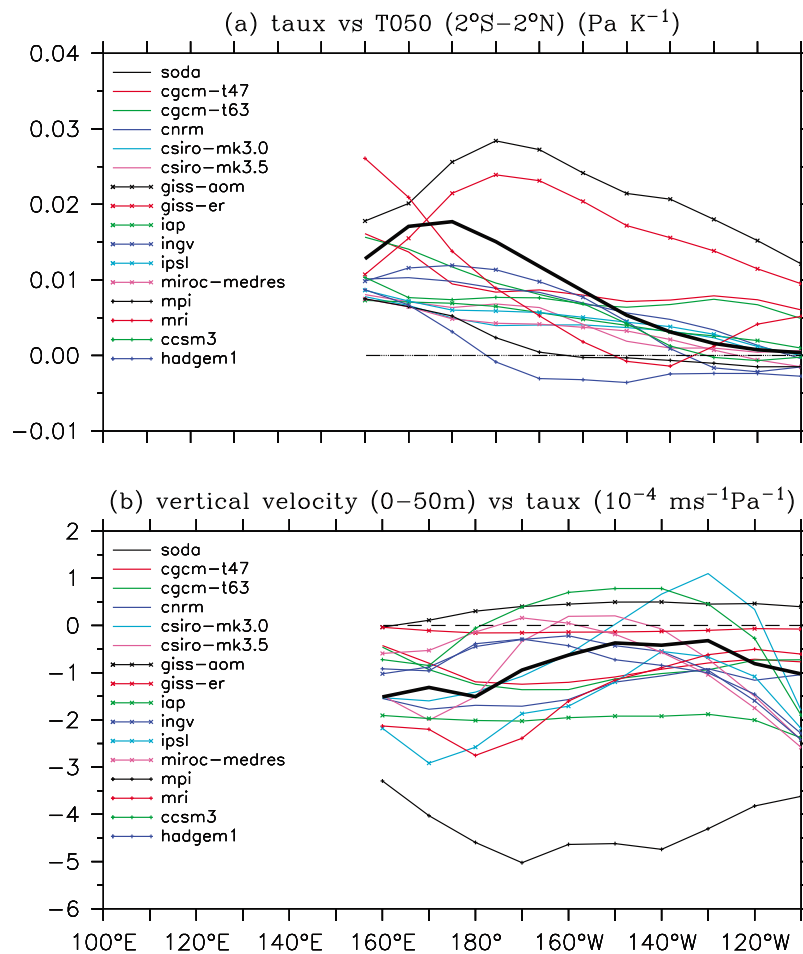


Figure 15. Linear regression of 2°S–2°N averaged of 20-year monthly mean data for (a) τ_x vs T050 (Pa K⁻¹) and (b) vertical velocity (0–50 m) vs τ_x ($\times 10^{-4}$ ms⁻¹ Pa⁻¹) from SODA ocean analysis and 15 IPCC AR4 CGCMs. The data are first converted to 10-degree bins in longitude before meridional averaging. The period for analysis is January 1980–December 1999.

advection (Figure 9a) due to overly strong vertical motion and vertical temperature gradient (Figures 12b and 12d). The cooling bias from the total heat advection has a magnitude similar to that of surface heat flux (Figure 6b). Thus, errors in both net surface heat flux and total heat advection contribute to cold SST bias along the equator. Our results suggest that the biases in the oceanic processes discussed here contribute to the eastern Pacific cold tongue bias.

[36] Bjerknes feedback analysis shows that almost all models underestimate the strength of Bjerknes feedback in the central and eastern Pacific between 160°E and 110°W (Figure 13), which may be related to insufficient surface zonal wind response to SST in the models and an erroneous subsurface temperature structure. An interesting result from the analysis of observations is that the horizontal heat advection, which is dominated by its zonal component, contributes more than the vertical advection does to the total advection. Therefore, the total heat advection, instead of the vertical heat advection, should be considered when discussing about Bjerknes feedback.

[37] The overly weak surface wind response to SST and the resultant overly weak Bjerknes feedback in the coupled models are surprising, since Lin [2007] found an excessive

surface wind response to SST for the atmospheric component of these coupled models forced by observed SST. Our finding suggests that coupling to an ocean model significantly reduces the excessive response of zonal winds to SST anomaly, which may be caused by the overly cold equilibrium SST along the equator and the erroneous ocean subsurface temperature structure. We hypothesize that the equatorial Pacific cold tongue bias in the coupled models is developed in two stages.

[38] Stage 1: In the initial state, both SST and the ocean temperature profile are similar to the observations in CGCMs. Next there is an overly strong Bjerknes feedback caused by the AGCMs' excessive surface zonal wind response to SST [Lin, 2007], which may be enhanced in some models by the excessive ocean upwelling response to trade winds (Figure 15b). Then the cold tongue becomes colder than the cold tongue in the observations.

[39] Stage 2: Eventually, when the cold tongue gets too cold (Figure 1), and the subsurface temperature structure becomes erroneous (Figure 14), the surface zonal wind response to SST becomes weaker (Figure 15a) and the Bjerknes feedback is significantly weakened. This bias is further enhanced by an erroneous ocean temperature structure

in most models. The Bjerknes feedback then becomes weaker than in the observations, and it no longer contributes to the excessive cold tongue.

[40] We plan to test these hypotheses in future studies using coupled model experiments initialized from the observed SST and ocean structure. *Zhang and Wang [2006]* did a pioneering study along this line with an emphasis on the role of the atmospheric model. More work is needed on the role of the ocean model and ocean–atmosphere feedback in the growth of the double-ITCZ pattern.

[41] **Acknowledgments.** We are greatly indebted to all those who contributed to the models and global data sets used in this study. Computational facilities have been provided by the National Oceanic and Atmospheric Administration (NOAA) and COAPS at the Florida State University. Yangxing Zheng is supported by NSF grant OCE-0453046. Toshiaki Shinoda is supported by NOAA CPO grant (GC10-400) under the Modeling, Analysis, and Prediction (MAP) Program, NSF grants OCE-0453046, AGS-0966844, and ATM-0745897, and 6.1 projects sponsored by the Office of Naval Research (ONR) under program element 601153 N. Jia-lin Lin is supported by NOAA CPO grant (GC10-400), by the National Aeronautics and Space Administration (NASA) under MAP program and by NSF grant ATM-0745872.

References

- Bellucci, A., S. Gualdi, and A. Navarra (2010), The double-ITCZ syndrome in coupled general circulation models: The role of large-scale vertical circulation regimes, *J. Clim.*, *23*, 1127–1145, doi:10.1175/2009JCLI3002.1.
- Bjerknes, J. (1969), Atmospheric teleconnections from the equatorial Pacific, *Mon. Weather Rev.*, *97*, 163–172, doi:10.1175/1520-0493(1969)097<0163:ATFTEP>2.3.CO;2.
- Bryden, H. L., and E. C. Brady (1985), Diagnostic model of the three-dimensional circulation in the upper equatorial Pacific Ocean, *J. Phys. Oceanogr.*, *15*, 1255–1273, doi:10.1175/1520-0485(1985)015<1255:DMOTTD>2.0.CO;2.
- Cai, M. (2003), Formation of the cold tongue and ENSO in the equatorial Pacific basin, *J. Clim.*, *16*, 144–155, doi:10.1175/1520-0442(2003)016<0144:FOTCTA>2.0.CO;2.
- Calvo, E., C. Pelejero, L. D. Pena, I. Cacho, and G. A. Logan (2011), Eastern equatorial Pacific productivity and related-CO₂ changes since the last glacial period, *Proc. Natl. Acad. Sci. USA*, *108*, 5537–5541, doi:10.1073/pnas.1009761108.
- Carton, J. A., and B. S. Giese (2008), A reanalysis of ocean climate using Simple Ocean Data Assimilation (SODA), *Mon. Weather Rev.*, *136*, 2999–3017, doi:10.1175/2007MWR1978.1.
- Carton, J. A., G. A. Chepurin, X. Cao, and B. S. Giese (2000a), A Simple Ocean Data Assimilation analysis of the global upper ocean 1950–1995, Part 1: Methodology, *J. Phys. Oceanogr.*, *30*, 294–309, doi:10.1175/1520-0485(2000)030<0294:ASODAA>2.0.CO;2.
- Carton, J. A., G. A. Chepurin, and X. Cao (2000b), A Simple Ocean Data Assimilation analysis of the global upper ocean 1950–1995, Part 2: Results, *J. Phys. Oceanogr.*, *30*, 311–326, doi:10.1175/1520-0485(2000)030<0311:ASODAA>2.0.CO;2.
- Clement, A. C., and R. Seager (1999), Climate and the tropical oceans, *J. Clim.*, *12*, 3383–3401, doi:10.1175/1520-0442(1999)012<3383:CATTO>2.0.CO;2.
- Clement, A. C., R. Seager, M. A. Cane, and S. E. Zebiak (1996), An ocean dynamical thermostat, *J. Clim.*, *9*, 2190–2196, doi:10.1175/1520-0442(1996)009<2190:AODT>2.0.CO;2.
- Clement, A. C., R. Seager, and R. Murtugudde (2005), Why are the tropical warm pools?, *J. Clim.*, *18*, 5294–5311, doi:10.1175/JCLI3582.1.
- Dai, A. G. (2006), Precipitation characteristics in eighteen coupled climate models, *J. Clim.*, *19*, 4605–4630, doi:10.1175/JCLI3884.1.
- Davey, M. K., et al. (2002), STOIC: A study of coupled model climatology and variability in tropical oceanic regions, *Clim. Dyn.*, *18*, 403–420, doi:10.1007/s00382-001-0188-6.
- Delecluse, P., M. Davey, Y. Kitamura, S. Philander, M. Suarez, and L. Bengtsson (1998), Coupled general circulation modeling of the tropical Pacific, *J. Geophys. Res.*, *103*, 14,357–14,373, doi:10.1029/97JC02546.
- Dijkstra, H. A., and J. D. Neelin (1995), Ocean-atmosphere interaction and the tropical climatology. Part II: Why the Pacific cold tongue is in the east, *J. Clim.*, *8*, 1343–1359, doi:10.1175/1520-0442(1995)008<1343:OAIATT>2.0.CO;2.
- Dijkstra, H. A., and J. D. Neelin (1999), Coupled process and the tropical climatology. Part III: Instabilities of the fully coupled climatology, *J. Clim.*, *12*, 1630–1643, doi:10.1175/1520-0442(1999)012<1630:CPATTC>2.0.CO;2.
- Fairall, C. W., E. F. Bradley, J. E. Hare, A. A. Grachev, and J. B. Edson (2003), Bulk parameterization of air-sea fluxes: Updates and verification for the COARE algorithm, *J. Clim.*, *16*, 571–591, doi:10.1175/1520-0442(2003)016<0571:BPOASF>2.0.CO;2.
- Field, C. B., M. J. Behrenfeld, J. T. Randerson, and P. Falkowski (1998), Primary production of the biosphere: Integrating terrestrial and oceanic components, *Science*, *281*, 237–240, doi:10.1126/science.281.5374.237.
- Frey, H., M. Latif, and T. Stockdale (1997), The coupled GCM ECHO-2. Part I: The tropical Pacific, *Mon. Weather Rev.*, *125*, 703–720, doi:10.1175/1520-0493(1997)125<0703:TCGEPI>2.0.CO;2.
- Jin, F.-F. (1996), Tropical ocean-atmosphere interaction, the Pacific cold tongue, and El Niño/Southern Oscillation, *Science*, *274*, 76–78, doi:10.1126/science.274.5284.76.
- Jones, P. W. (1999), First- and second-order conservative remapping schemes for grids in spherical coordinates, *Mon. Weather Rev.*, *127*, 2204–2210, doi:10.1175/1520-0493(1999)127<2204:FASOCR>2.0.CO;2.
- Kalnay, E., et al. (1996), The NCEP/NCAR 40-year reanalysis project, *Bull. Am. Meteorol. Soc.*, *77*, 437–471, doi:10.1175/1520-0477(1996)077<0437:TNYRP>2.0.CO;2.
- Large, W. G., J. C. McWilliams, and S. C. Doney (1994), Oceanic vertical mixing: Review and model with a nonlocal boundary layer parameterization, *Rev. Geophys.*, *32*, 363–403, doi:10.1029/94RG01872.
- Latif, M., et al. (2001), ENSIP: The El Niño simulation intercomparison project, *Clim. Dyn.*, *18*, 255–276, doi:10.1007/s003820100174.
- Lin, J.-L. (2007), The double-ITCZ problem in IPCC AR4 coupled GCMs: Ocean-atmosphere feedback analysis, *J. Clim.*, *20*, 4497–4525, doi:10.1175/JCLI4272.1.
- Liu, Z. (1997), Oceanic regulation of the atmospheric Walker circulation, *Bull. Am. Meteorol. Soc.*, *78*, 407–412, doi:10.1175/1520-0477(1997)078<0407:OROTAW>2.0.CO;2.
- Liu, Z., and B. Huang (1997), A coupled theory of the tropical climatology: Warm pool, cold tongue, and Walker circulation, *J. Clim.*, *10*, 1662–1679, doi:10.1175/1520-0442(1997)010<1662:ACTOTC>2.0.CO;2.
- Luo, J. J., S. Masson, E. Roeckner, G. Madec, and T. Yamagata (2005), Reducing climatology bias in an ocean-atmosphere CGCM with improved coupling physics, *J. Clim.*, *18*, 2344–2360, doi:10.1175/JCLI3404.1.
- Mechoso, C. R., et al. (1995), The seasonal cycle over the tropical Pacific in coupled ocean-atmosphere general circulation models, *Mon. Weather Rev.*, *123*, 2825–2838, doi:10.1175/1520-0493(1995)123<2825:TSCOTT>2.0.CO;2.
- Meehl, G. A., C. Covey, B. McAvaney, M. Latif, and R. J. Stouffer (2005), Overview of the Coupled Model Intercomparison Project, *Bull. Am. Meteorol. Soc.*, *86*, 89–93, doi:10.1175/BAMS-86-1-89.
- Misra, V., L. Marx, M. Brunke, and X. Zeng (2008), The equatorial Pacific cold tongue bias in a coupled climate model, *J. Clim.*, *21*, 5852–5869, doi:10.1175/2008JCLI2205.1.
- Neelin, J. D., and H. A. Dijkstra (1995), Ocean-atmosphere interaction and the tropical climatology. Part I: The dangers of flux correction, *J. Clim.*, *8*, 1325–1342, doi:10.1175/1520-0442(1995)008<1325:OAIATT>2.0.CO;2.
- Neelin, J. D., et al. (1992), Tropical air-sea interaction in general circulation models, *Clim. Dyn.*, *7*, 73–104, doi:10.1007/BF00209610.
- Peters, M. E., and C. S. Bretherton (2005), A simplified model of the Walker circulation with an interactive ocean mixed layer and cloud-radiative feedback, *J. Clim.*, *18*, 4216–4234, doi:10.1175/JCLI3534.1.
- Ramanathan, V., and W. Collins (1991), Thermodynamic regulation of ocean warming by cirrus clouds deduced from observations of the 1987 El Niño, *Nature*, *351*, 27–32, doi:10.1038/351027a0.
- Randall, D. A., et al. (2007), Climate models and their evaluation, in *Climate Change 2007: The Physical Science Basis*, edited by S. Solomon et al., pp. 591–648, Cambridge Univ. Press, Cambridge, U. K.
- Simmons, A. J., and J. K. Gibson (2002), The ERA-40 Projects Plan, Series #1, 63pp., Eur. Cent. for Medium-Range Weather Forecasts, Reading, U. K.
- Smith, R. D., J. K. Dukowicz, and R. C. Malone (1992), Parallel ocean general circulation modeling, *Physica D*, *60*, 38–61, doi:10.1016/0167-2789(92)90225-C.
- Song, X., and G. J. Zhang (2009), Convection parameterization, tropical Pacific double ITCZ, and upper-ocean biases in the NCAR CCSM3. Part I: Climatology and atmospheric feedback, *J. Clim.*, *22*, 4299–4315, doi:10.1175/2009JCLI2642.1.
- Sun, D.-Z., and Z. Liu (1996), Dynamic ocean-atmosphere coupling: A thermostat for the tropics, *Science*, *272*, 1148–1150, doi:10.1126/science.272.5265.1148.
- Swenson, M. S., and D. V. Hansen (1999), Tropical Pacific ocean mixed layer heat budget: The Pacific cold tongue, *J. Phys. Oceanogr.*, *29*, 69–81, doi:10.1175/1520-0485(1999)029<0069:TPOMLH>2.0.CO;2.

- van der Vaart, P. C. F., H. A. Dijkstra, and F.-F. Jin (2000), The Pacific cold tongue and the ENSO mode: A unified theory within the Zebiak-Cane model, *J. Atmos. Sci.*, *57*, 967–988, doi:10.1175/1520-0469(2000)057<0967:TPCTAT>2.0.CO;2.
- Wallace, J. M. (1992), Effect of deep convection on the regulation of tropical sea surface temperature, *Nature*, *357*, 230–231, doi:10.1038/357230a0.
- Wittenberg, A. T., A. Rosati, N. C. Lau, and J. J. Plushay (2006), GFDL's CM2 Global coupled climate models. Part III: Tropical Pacific climate and ENSO, *J. Clim.*, *19*, 698–722, doi:10.1175/JCLI3631.1.
- Wyrtki, K. (1981), An estimate of equatorial upwelling in the Pacific, *J. Phys. Oceanogr.*, *11*, 1205–1214, doi:10.1175/1520-0485(1981)011<1205:AEOEUI>2.0.CO;2.
- Yu, J.-Y., and C. R. Mechoso (1999), Links between annual variations of Peruvian stratocumulus clouds and of SST in the eastern equatorial Pacific, *J. Clim.*, *12*, 3305–3318, doi:10.1175/1520-0442(1999)012<3305:LBAVOP>2.0.CO;2.
- Yu, L., and R. A. Weller (2007), Objectively analyzed air-sea fluxes for the global ice-free oceans (1981–2005), *Bull. Am. Meteorol. Soc.*, *88*, 527–539, doi:10.1175/BAMS-88-4-527.
- Yu, L., X. Jin, and R. A. Weller (2008), Multidecade global flux datasets from the objectively analyzed air-sea fluxes (OAFflux) Project: Latent and sensible heat fluxes, ocean evaporation, and related surface meteorological variables, *OAFflux Project Tech. Rep. OA-200801*, 64pp., Woods Hole Oceanogr. Inst., Woods Hole, Mass.
- Zhang, G. J., and X. Song (2010), Convection parameterization, tropical Pacific double ITCZ, and upper-ocean biases in the NCAR CCSM3. Part II: Coupled feedback and the role of ocean heat transport, *J. Clim.*, *23*, 800–812, doi:10.1175/2009JCLI3109.1.
- Zhang, G. J., and H. Wang (2006), Toward mitigating the double ITCZ problem in NCAR CCSM3, *Geophys. Res. Lett.*, *33*, L06709, doi:10.1029/2005GL025229.
- Zhang, Y.-C., W. B. Rossow, A. A. Lacis, V. Oinas, and M. I. Mishchenko (2004), Calculation of radiative fluxes from the surface to top of atmosphere based on ISCCP and other global data sets: Refinements of the radiative transfer model and the input data, *J. Geophys. Res.*, *109*, D19105, doi:10.1029/2003JD004457.
- Zheng, Y., and B. S. Giese (2009), Ocean heat transport in Simple Ocean Data Assimilation: Structure and mechanisms, *J. Geophys. Res.*, *114*, C11009, doi:10.1029/2008JC005190.
- Zheng, Y., T. Shinoda, G. N. Kiladis, J.-L. Lin, E. J. Metzger, H. E. Hurlburt, and B. S. Giese (2010), Upper-ocean processes under the stratus cloud deck in the southeast Pacific Ocean, *J. Phys. Oceanogr.*, *40*, 103–120, doi:10.1175/2009JPO4213.1.
- Zheng, Y., T. Shinoda, J.-L. Lin, and G. N. Kiladis (2011), Sea surface temperature biases under the stratus cloud deck in the southeast Pacific Ocean in 19 IPCC AR4 coupled general circulation models, *J. Clim.*, *24*, 4139–4164, doi:10.1175/2011JCLI4172.1.